Available online at www.sciencedirect.com
SCIENCE DIRECT®
Cement & Concrete Composites 28 (2006) 246–255
Cement & Concrete Composites
www.elsevier.com/locate/cemconcomp

Corrosion behaviour in concrete of three differently galvanized steel bars

T. Bellezze *, M. Malavolta, A. Quaranta, N. Ruffini, G. Roventi

Dipartimento di Fisica ed Ingegneria dei Materiali e del Territorio, Università Politecnica delle Marche, Via Brecce Bianche, 60131 Ancona, Italy

Abstract

The increasing use of galvanized steel reinforcements in concrete structures submitted to aggressive environments induces research into innovative zinc coatings with higher corrosion resistance. In this work, several cylindrical concrete specimens were manufactured with two cements of different alkalinity and reinforced with different hot-dip galvanized bars obtained from the ''traditional'' Zn–Pb bath and from two ''modified baths'': Zn–Ni–Bi and Zn–Ni–Sn–Bi. The corrosion rate and corrosion potential of the bars were monitored during the air curing period and during wet–dry exposure both in tap water and in a 5% sodium chloride solution. The results showed that the coatings obtained from Zn–Ni–Sn–Bi bath have the highest corrosion rates, when the aggressiveness of the concrete matrix is determined mainly by its alkalinity. On the contrary, when the corrosion process is determined mainly by the penetration of chlorides (concrete manufactured with cement having a low alkali content) Zn–Ni–Sn–Bi was attacked only when the chloride concentration at the concrete cover depth reached the threshold of 4.02% (by weight of cement), which is higher than those necessary for the attack of the other coatings studied (1.36% for Zn–Ni–Bi, 1.73% for Zn–Pb).

Keywords: Galvanized steel; Alloying elements; Corrosion in concrete; Chlorides exposure

1. Introduction

The production of zinc coatings with a good ''quality-cost'' ratio [1] means a low zinc consumption during the process and the obtainment of coatings with controlled thickness and good corrosion resistance. Coating quality and zinc consumption in hot-dip galvanizing strongly depend on the zinc–iron reactivity and on the drainage of zinc from workpieces during their withdrawal. The zinc–iron reactivity is mainly influenced by the silicon and phosphorus steel content [2]; zinc drainage, instead, is influenced by bath fluidity [3]. Therefore, some alloying elements are added to the molten zinc bath in order to limit the zinc–iron reactivity and to improve the bath fluidity. In particular, lead additions (usually, about 1%) were extensively used because it gives a more fluid molten zinc bath; however, this metal is considered hazardous to the environment, so new baths with different alloying elements have been proposed, such as Zn–Ni–Bi [1] or Zn–Ni–Sn–Bi. Nickel additions to the molten bath reduces zinc–iron reactivity while maintaining the specification minima for coating thickness [4]. Tin also reduces zinc–iron reactivity and is commonly used in combination with nickel [5]. All these ''modified baths'' with respect to the Zn–Pb ''traditional bath'' have been mainly developed in order to decrease zinc–iron reactivity and to reduce the coating thickness. Furthermore, the corrosion resistance in the concrete matrix of the coatings obtained with these baths is gaining interest [4] because the initial cost for galvanizing could be lower than that of restoring during the service life [6]. In Italy, the use of galvanized steel is becoming important because a recent technical normative on constructions recommends the use of these reinforcements in particularly aggressive environments, as in the presence of chloride contamination, especially when the concrete cover is cracked. The interaction between galvanized steel and various alkaline solutions, with and without $Ca(OH)_2$ has been widely studied [7–11]; the interaction between galvanized bars

* Corresponding author. Tel.: +39 071 2204727; fax: +39 071 2810327.
E-mail address: tizbel@ascu.unian.it (T. Bellezze).

0958-9465/$ - see front matter © 2006 Elsevier Ltd. All rights reserved.
doi:10.1016/j.cemconcomp.2006.01.011

and concrete matrixes obtained with different cements has been studied in the past by other researchers [4,12] and by the present authors [13,14].

The aim of this work was to study the corrosion resistance of reinforcements galvanized with Zn–Ni–Bi and with Zn–Ni–Sn–Bi "modified baths", with respect to reinforcements galvanized with the Zn–Pb "traditional bath" and to a pure zinc rod, where the effect of the alloying elements and of the zinc–iron alloys, typical of the galvanized coatings is absent. Cylindrical concrete specimens were manufactured and reinforced with galvanized bars and with a pure zinc rod; two cements with a different alkali content were used to study the effect of alkalinity of the concrete matrix on the behaviour of the reinforcements. After the air curing period, the concrete specimens were submitted to wet–dry exposure both in tap water and in a 5% sodium chloride solution. The corrosion rate and the corrosion potential of the bars were monitored during the air curing period and during the wet–dry exposure.

2. Experimental details

Several cylindrical specimens ($\phi = 16$ cm; height = 12.5 cm) (Fig. 1) similar to those used in a previous work [15] were manufactured. Two 52.5 R Portland cements (Table 1) were used: the first one, labelled "L", develops less alkalinity than the second one, labelled "P", in the concrete matrix in wet conditions. Both for L and P cement the mix design reported in Table 2 was used.

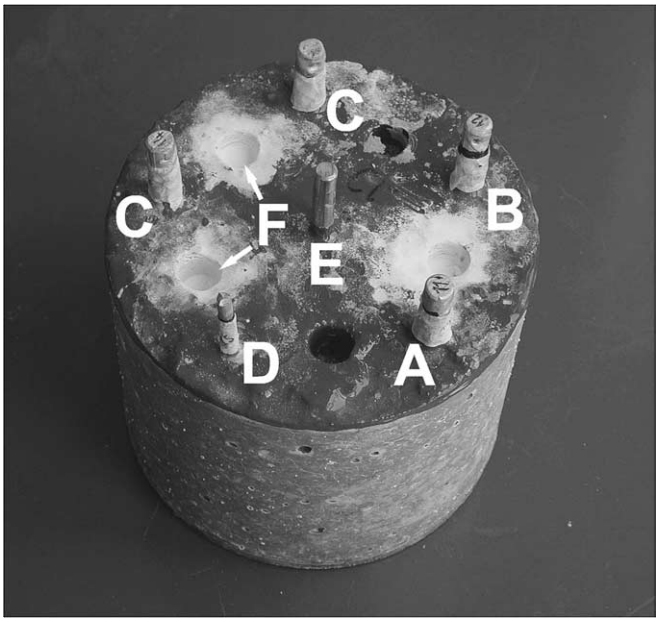

Fig. 1. Concrete reinforced specimen: (A) bar galvanized in the Zn–Pb bath; (B) bar galvanized in the Zn–Ni–Bi bath; (C) bars galvanized in the Zn–Ni–Sn–Bi bath; (D) pure Zn rod; (E) counter electrode; (F) pits for placing the reference electrode.

Table 2
Mix design relative to 1 m^3 of concrete (water–cement ratio = 0.55)

Water	3.02 kg
Cement	5.48 kg
Sand ($D_{max} = 4$ mm)	7.88 kg
Gravel ($D_{max} = 8$ mm)	11.81 kg

Table 3
Composition of the baths used for hot-dip galvanizing of the bars

Bath	Label	Pb (%)	Bi (%)	Sn (%)	Ni (%)	Al (%)
Zn–Pb	A	1 (Saturated)	–	–	–	–
Zn–Ni–Bi	B	–	0.15	–	0.05	0.004
Zn–Ni–Sn–Bi	C	–	0.1	1.1	0.05	0.007

Each specimen was reinforced with four galvanized ribbed steel bars ($\phi = 10$ mm; length = 12 cm) and one pure zinc rod ($\phi = 5$ mm; length = 12 cm), used for comparison (Fig. 1). Considering the silicon and the phosphorous content of the steel used, which was respectively 0.14% and 0.0015 wt%, it can be classified as a "hyper-Sandelin" steel [2]: its reactivity with respect to molten zinc during the hot-dip galvanizing may be considered high. Before hot-dip galvanizing, each bar sample was pretreated as described previously [1]. After the pretreatments, the bars were galvanized ($T = 444 \pm 1$ °C, time = 6 min, air cooling) in three different baths having the composition reported in Table 3. For all the bars and the zinc rods, the concrete cover was 1.5 cm. In the centre of each concrete specimen, a stainless steel rod was embedded and used as counter electrode during polarization resistance measurements. The pits visible in Fig. 1 on the top of the concrete specimens were produced for placing the saturated calomel electrode (SCE) used as reference electrode. An epoxy resin was applied on the top and on the bottom of the concrete cylinders (Fig. 1) to limit the penetration of aqueous solutions from the only lateral surface. The epoxy resin was not applied on the pits described above in order to keep the electric contact for the reference electrode during the electrochemical measurements free. During wetting tests, the solution level was maintained slightly under the top of the concrete specimen to avoid the penetration of the solution in the pits. Each bar sample, before embedding in the concrete specimen, was suitably shielded with an epoxy

Table 1
Chemical composition of the cements used

Cement type	Loss on ignition	SiO_2	Al_2O_3	Fe_2O_3	CaO	MgO	SO_3	Na_2O	K_2O	Insoluble residue	Free lime	C_3A	C_4AF
L	1.80	21.90	3.30	5.10	62.50	2.70	2.10	0.30	0.40	0.90	1.40	0.20	15.50
P	3.26	21.83	3.41	0.23	65.41	1.67	2.70	0.69	0.37	0.54	1.01	8.64	0.70

Table 4
Summary of the bars embedded in the different concrete specimens and submitted to the different exposure conditions

Reinforcements for each concrete specimen	Labels (28 days of air curing)	Wetting conditions (wet–dry cycles exposure (22 cycles))	Labels
Cement type L (two concrete specimens)			
One bar obtained from bath A	AL	Tap water (W)	ALW
One bar obtained from bath B	BL		BLW
Two bars obtained from bath C	CL		CLW
One pure zinc rod D	DL		DLW
Cement type L (two concrete specimens)			
One bar obtained from bath A	AL	NaCl 5% solution (Cl)	ALCl
One bar obtained from bath B	BL		BLCl
Two bars obtained from bath C	CL		CLCl
One pure zinc rod D	DL		DLCl
Cement type P (two concrete specimens)			
One bar obtained from bath A	AP	Tap water (W)	APW
One bar obtained from bath B	BP		BPW
Two bars obtained from bath C	CP		CPW
One pure zinc rod D	DP		DPW
Cement type P (two concrete specimens)			
One bar obtained from bath A	AP	NaCl 5% solution (Cl)	APCl
One bar obtained from bath B	BP		BPCl
Two bars obtained from bath C	CP		CPCl
One pure zinc rod D	DP		DPCl

The labels shown are those used in the plots.

resin in order to expose a defined surface area equal to 22 cm^2. In the case of the pure zinc rod, the exposed surface was 11 cm^2.

Table 4 summarizes all the bar samples and the zinc rods embedded in the different concrete specimens with their corresponding labels.

Concrete specimens were demoulded after 1 day and subsequently, after 28 days of air curing (R.H. = 60%), submitted to wet-cycles with tap water or in a 5% NaCl solution; a wet–dry cycle consisted in 1 day of wetting and 6 days of drying.

Corrosion potential (E_{corr}) was measured with a high impedance digital multimeter, while the polarization resistance (R_p) measurement was performed by means of a three-electrode configuration using an Amel workstation (566 function generator; 549 potentiostat; 621 differential electrometer) managed by a software suitably developed using Lab Windows and the Acquisition Board NI AT-MIO-16 (12 bit, 100 ksample/s). R_p was measured with the following method: starting from E_{corr}, a galvanodynamic polarization (0.5 μA/s) was begun in the cathodic direction and interrupted when a value of 5 mV more cathodic than E_{corr} was reached. After polarization, the sample was allowed to stabilise again at the initial E_{corr} value; an anodic scan (0.5 μA/s) was then performed from E_{corr} until a value of 5 mV more positive was reached. R_p was obtained by calculating the average value of the slopes of the two potential/current curves. From the R_p value, the corrosion current i_{corr} was calculated using the classical Stern–Geary equation [16], considering $B = 26$ mV [17,18]; then, according to Faraday's first law, the corrosion rate v_{corr} (μm/year) was calculated. The data were obtained by calculating the average of the E_{corr} and v_{corr} values related to the bars tested in the same experimental conditions (Table 4). The dispersion of the data was controlled by calculation of the standard deviation which resulted fairly reduced, except during the transition of the galvanized bars and pure zinc rods from active to passive state just after the cast, as described in the next section. The experimentation went on up to the 22nd wet–dry cycle.

To characterize the coatings and to study the morphology of the corrosive attack, metallographic analysis was performed on some galvanized bars before embedding in the concrete and on those removed from the concrete specimens after the exposure tests. The bars were cross-sectioned, polished and submitted to a chemical attack performed with Nital 2 (2% of 69% HNO_3 in ethyl alcohol); an optical microscope Leitz Laborlux 12 POL S was used.

The chloride concentration at concrete cover depth was obtained by means of powder analysis on some non reinforced specimens, manufactured with the same procedure as the reinforced ones, submitted to the same exposure conditions. Every three wet–dry cycles, the non-reinforced specimens were drilled with a 16 mm diameter bit in the lateral surface up to 1 cm of depth, the powder produced was discarded and the specimen drilled again from 1 to 2 cm of depth, this time accurately collecting the powder produced. The powder (about 5 g) was mixed with 40 ml of distilled water and stirred for 24 h with a magnetic stirrer. After the filtration, the water was analyzed by means of Ionic Chromatograph Dionex Mod. DX120 and the percentage

of chlorides by weight of cement was calculated. This value was assumed as the chlorides content in correspondence of the concrete cover (1.5 cm).

At the end of wet–dry exposure, in order to obtain the chlorides penetration depth, the following technique was used. The reinforced and non-reinforced concrete specimens were broken in two halves and each internal surface was submitted to spraying once with a 6% NaOH solution, then to spraying five times with 1 g dm^{-3} of fluorescein alcoholic solution and finally to spraying twice with a 0.1 M $AgNO_3$ solution. After each spraying, complete drying of the specimens was assured. After this procedure, on the internal surface of each half, it was possible to measure the distance between the external specimen surface and the border between the dark middle area (absence of chlorides) and the two lighter external areas (presence of chlorides). The average of the distances measured for the specimens in the same experimental conditions was calculated.

3. Results

3.1. Microstructure analysis of the non-corroded zinc coatings

Fig. 2 shows the microstructure of the zinc coatings studied. The average thickness for the Zn–Pb, Zn–Ni–Bi and Zn–Ni–Sn–Bi coatings is 215, 151 and 130 μm, respectively. Considering that the steel is hyper-Sandelin, these values indicate that the Zn–Fe reaction during hot-dip galvanizing is kinetically controlled in the two "modified baths" B (Zn–Ni–Bi, Fig. 2b) and C (Zn–Ni–Sn–Bi, Fig. 2c) with respect to the "traditional bath" A (Zn–Pb, Fig. 2a). The coating obtained with Zn–Pb bath could be considered quite anomalous because some zones typical of non-reactive steel (presence of δ phase) are visible. For the coating obtained from Zn–Ni–Sn–Bi bath, the η phase was not well defined as that of the coating obtained with Zn–Ni–Bi bath, because the ζ phase is dispersed in η phase.

3.2. Electrochemical measurements

From now on, the specimens manufactured with cement "L" and those manufactured with cement "P" will be briefly indicated "specimens L" and "specimens P", respectively.

Just after the cast, the bars embedded in the specimens L assume a typical active potential (−1350 to −1450 mV vs SCE, Fig. 3a) which starts to move slowly toward passive values after about 6 h. At the same time, the corrosion rates are very high (150–300 μm/year) for all samples (Fig. 3b). After 1 day from the cast, all the bars became passive and the potentials reach values around −650 mV; contemporarily, the corrosion rate decreases under 20 μm/year. During the whole air curing period, the potentials continue to become more positive (from −700/−600 mV to −500/−400 mV vs SCE) and the corrosion rates decrease below 6 μm/year (data not shown). During this period, the pure zinc rod showed the lowest corrosion rate with respect to the galvanized bars.

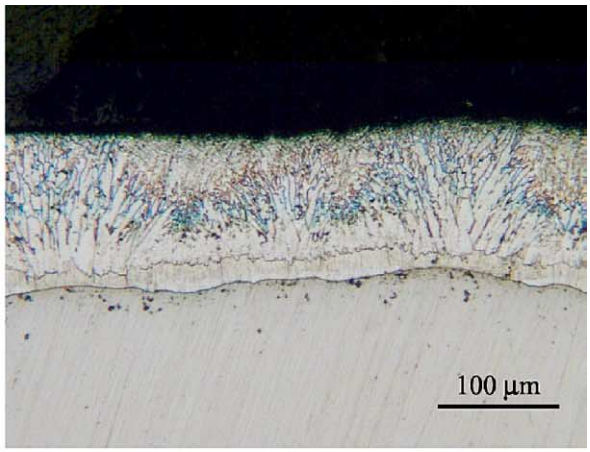

(a)

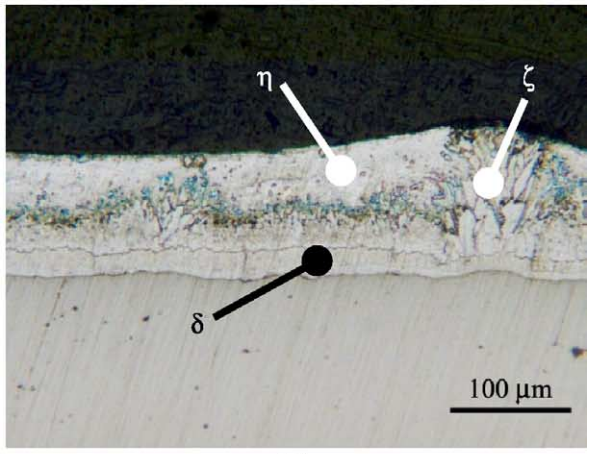

(b)

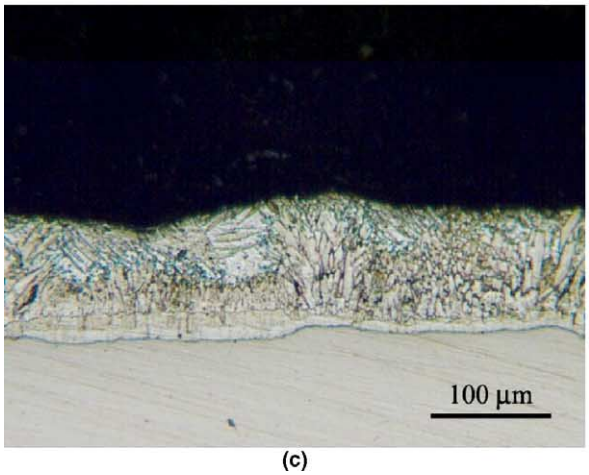

(c)

Fig. 2. Microstructure of the zinc coatings on the hot-dip galvanized bars obtained with the following baths: (a) Zn–Pb; (b) Zn–Ni–Bi; (c) Zn–Ni–Sn–Bi.

Just after the cast, only part of the bars embedded in the specimens P are in the active state (Fig. 4a), while the others assume a potential close to −900 mV vs SCE and become active after 1 day (potential close to −1350 mV). After two days from the cast, the bars embedded in the

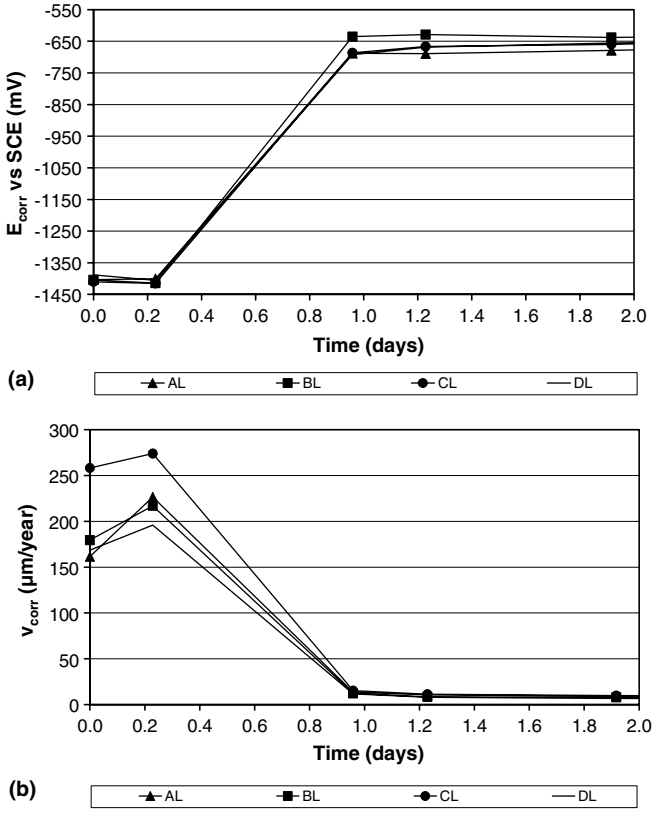

Fig. 3. Corrosion potential (a) and corrosion rate (b) trends relative to the bars embedded in specimens L during the first period after the cast.

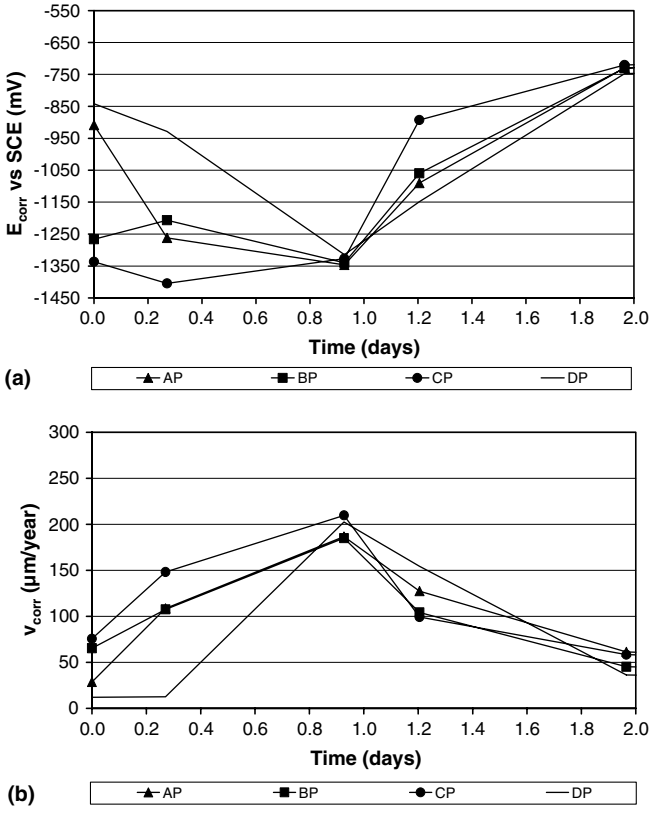

Fig. 4. Corrosion potential (a) and corrosion rate (b) trends relative to the bars embedded in specimens P during the first period after the cast.

specimens P reach a corrosion rate around 50 μm/year (Fig. 4b). On prolonging the air curing period, as observed for the bars embedded in the specimens L, even the corrosion potentials of the bars embedded in the specimens P become more positive, from −750/−700 mV to −550/−450 mV vs SCE; during the same period, the corrosion rates decrease from around 50 μm/year to around 12 μm/year (data not shown). The pure zinc rod showed the lowest corrosion rate with respect to the galvanized bars.

It is noteworthy that, just after the cast, the bars galvanized in the Zn–Ni–Sn–Bi bath appear particularly affected by the alkalinity of the concrete matrix and therefore they are the ones with the highest corrosion rate (Figs. 3b and 4b, curves CL and CP).

Figs. 5 and 6 show the corrosion rate values related to the bars embedded in the L and P concrete specimens respectively, during the wet–dry exposure. The "positive peaks" in Figs. 5 and 6 correspond to the values of corrosion rates obtained during the wetting periods, indicated by the horizontal dotted line on the top of each plot. The increase in the corrosion rates of the bars galvanized in the Zn–Ni–Bi bath, embedded in the specimens L and submitted to wet–dry cycles with 5% NaCl solution (Fig. 5a, curve BLCl), indicate that the localized corrosion attack starts from the 3rd wet–dry cycle. The initiation of the localized attack is caused by the damage of the passive film, due to the chloride ions [12], which reach a critical percentage (1.36% by weight of cement) in correspondence of the concrete cover depth. The same corrosion initiation is slightly delayed for the bars galvanized in the traditional Zn–Pb bath: their corrosion rate starts to increase after the 6th cycle when the chlorides concentration reaches the value of 1.73% (Fig. 5a, curve ALCl). The bars galvanized in the Zn–Ni–Sn–Bi bath show the best corrosion resistance because the chloride level necessary for the increase in the corrosion rate is very high: 4.02% after the 12th cycle (Fig. 5a, curve CLCl). For the same specimens L during the wet–dry exposure with tap water (Fig. 5b), the "positive peaks" related to corrosion in wetting conditions are subjected to a "damping phenomenon" toward the end of the exposure: higher corrosion rates can be observed during the early cycles, while lower corrosion rates are obtained on increasing the cycles number. On approaching the end of the wet–dry cycles in tap water, the corrosion rates range around 5 μm/year.

Both during wet–dry cycles in NaCl solution, before the chlorides attack, and during wet–dry cycles in tap water, the bars galvanized with the Zn–Ni–Sn–Bi bath showed the highest corrosion rate (Fig. 5, curves CLCl and CLW). The results obtained also show that the corrosion rates of the pure zinc rod are lower than those of the galvanized bars. The corrosion potential during the wet–dry exposure (results not shown) ranged between −500 and −700 mV vs SCE, when the coatings were in the passive state, while values around −800 mV were reached when the attack promoted by chloride ions initiated.

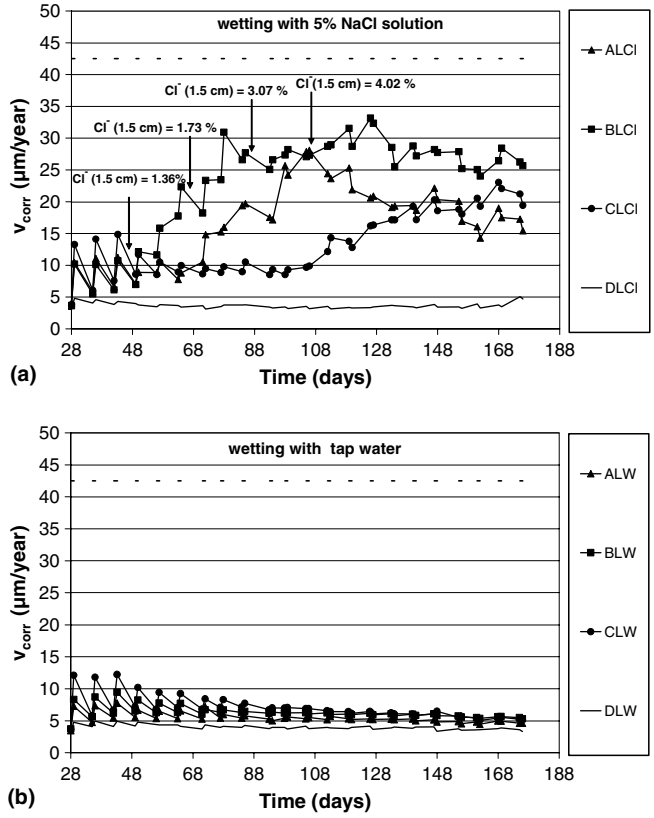

Fig. 5. Corrosion rate (v_{corr}) of the bars embedded in the concrete specimens manufactured with cement L during the exposure to wet–dry cycles in 5% NaCl solution (a) and in tap water (b). The percentage of chloride ions by weight of cement are indicated in the diagram (a) in correspondence of the concrete cover depth (1.5 cm) and in correspondence of the 3rd, 6th, 9th and 12th cycle.

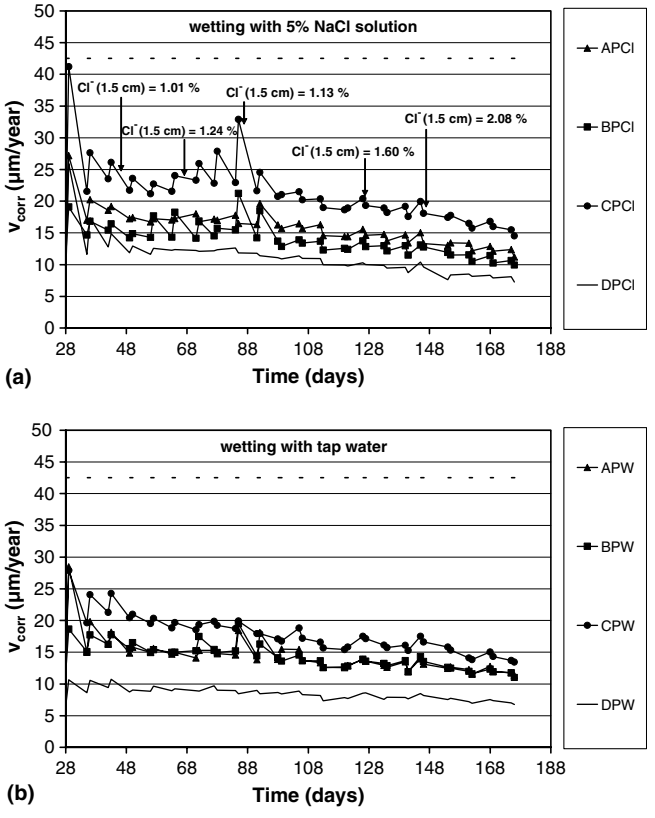

Fig. 6. Corrosion rate (v_{corr}) of the bars embedded in the concrete specimens manufactured with the cement P during the exposure to wet–dry cycles in 5% NaCl solution (a) and in tap water (b). The percentage of chloride ions by weight of cement are indicated in the diagram (a) in correspondence of the concrete cover depth (1.5 cm) and in correspondence of the 3rd, 6th, 9th, 15th and 18th cycle.

Fig. 6 shows the corrosion rate values related to the bars embedded in the specimens P. The percentages of chlorides found in correspondence of the concrete cover for specimens P (Fig. 6a) were lower than those relative to specimens L (Fig. 5a) at the same number of cycles, while the increase in the corrosion rates due to the localized corrosion promoted by chlorides attack was not observed. It is noteworthy that the corrosion rates related to the galvanized bars embedded in the specimens P are higher than those of the bars embedded in the specimens L, before the achievement of the critical threshold of chlorides concentration for these last ones. In particular, the Zn–Ni–Sn–Bi galvanized bars in the specimens P show the highest corrosion rates (Fig. 6a, curve CPCl). Instead, for the whole exposure period during wet–dry cycles with tap water, the corrosion rates of all bars embedded in the specimens P (Fig. 6b) were higher than those of the correspondent bars embedded in the specimens L (Fig. 5b); even in this case the Zn–Ni–Sn–Bi bars show the highest corrosion rates (Fig. 6b, curve CPW). The pure zinc rod shows the lowest corrosion rates in specimens P as too. During the wet–dry exposure, the corrosion potential of the galvanized bars in specimens P ranged in the common passive regions (−500 to −700 mV).

3.3. Chlorides penetration depth obtained by the $AgNO_3$ spraying test

Fig. 7 shows an histogram with the results obtained from the $AgNO_3$ spraying test performed as described

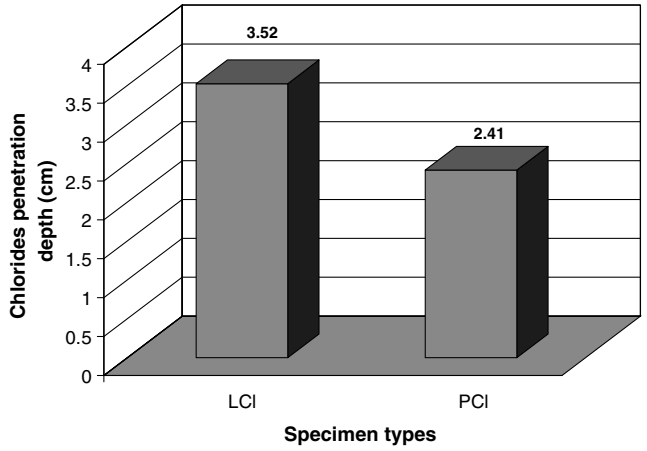

Fig. 7. Average chlorides penetration depth on the internal surface of the concrete L and P specimen halves obtained by the $AgNO_3$ spraying test.

previously in Section 2. The average values of the chlorides penetration depth indicate that they penetrate more deeply in specimens L with respect to specimens P. This result confirms the higher penetration of chlorides in the less alkaline concrete matrix, as demonstrated by the concentration values reported in Figs. 5a and 6a.

3.4. Microstructure analysis of the zinc coatings after wet–dry exposure

The microstructure of the galvanized bars after wet–dry exposure in NaCl solution (Fig. 8) shows that the chlorides attack was more severe in the bars embedded in specimens

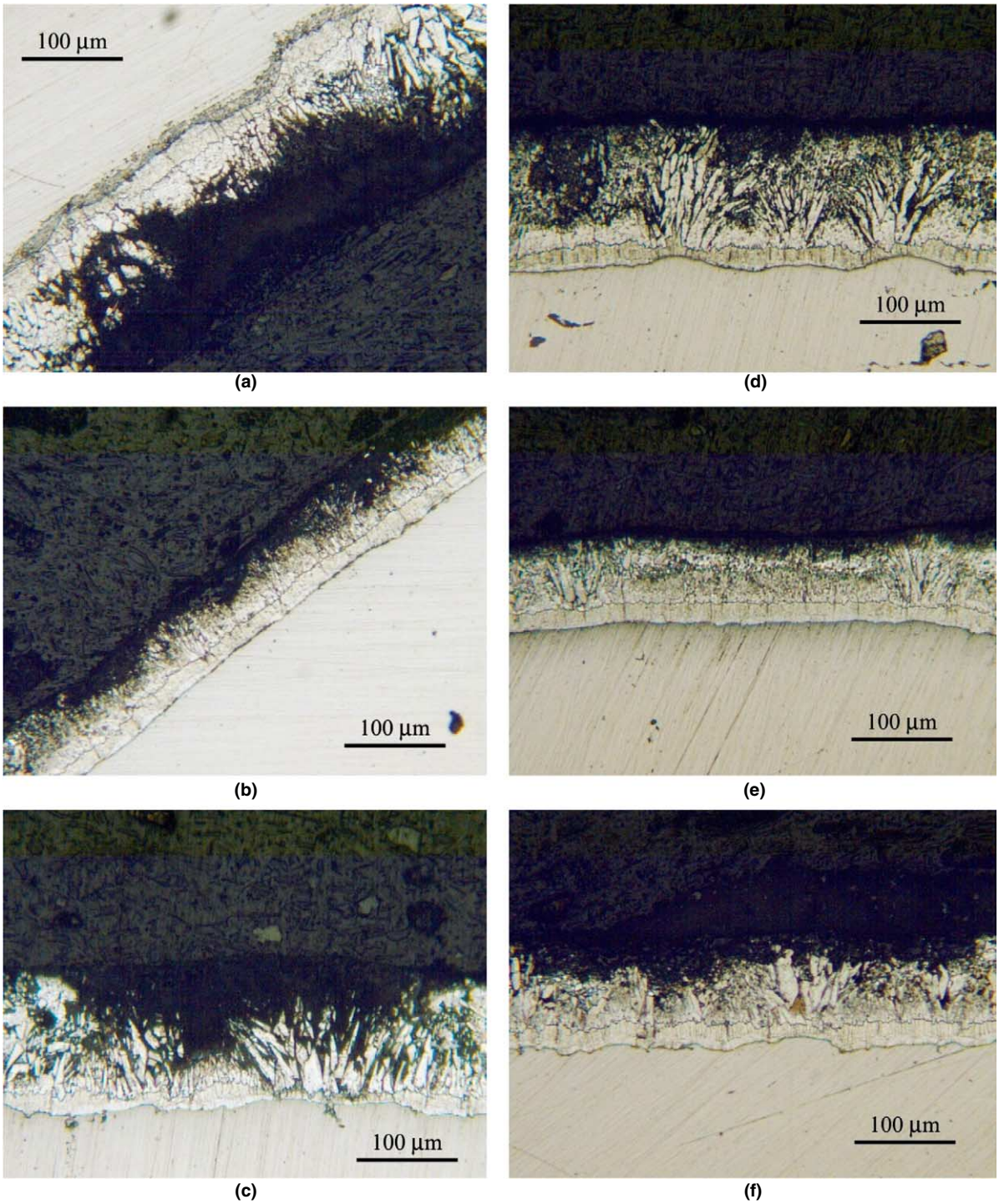

Fig. 8. Metallographic characterization of the zinc coatings after wet–dry exposure in NaCl: (a) Zn–Pb, specimens L; (b) Zn–Ni–Bi, specimens L; (c) Zn–Ni–Sn–Bi, specimens L; (d) Zn–Pb, specimens P; (e) Zn–Ni–Bi, specimens P; (f) Zn–Ni–Sn–Bi, specimens P.

L (Fig. 8a–c) with respect to that observed on the bars embedded in specimens P (Fig. 8d–f).

After the wet–dry exposure in tap water (images not shown), a corrosion attack less severe than that obtained in chloride solution was observed; in particular, the corrosion attack was not severe for the bars embedded in specimens L, while a higher and uniform corrosion was observed for galvanized bars embedded in specimens P. In all cases the η phase was not completely consumed.

4. Discussion

The behaviour of galvanized steel in alkaline aqueous solutions [4,7–12,17] and in concrete matrix [4,12–15,17] is fairly known and, in particular, the corrosion potentials corresponding to "active state" and "passive state" of the zinc coatings with reference to the "decomposition line of water" in the zinc Pourbaix's diagram are known [9].

In the early contact of galvanized bars and zinc rod with the alkaline concrete matrix, corrosion potentials under −1000 mV vs SCE and very high corrosion rates, due to the active corrosion of zinc (Figs. 3a,b, and 4a,b), were found. The difference in the activation of the bars embedded in the two types of concrete specimens could be explained with the different solubility of the alkali present in the two cements used. This could be in agreement with the delay of the complete activation of the bars embedded in specimens P (after about 20 h; see Fig. 4). After about 1 day, the corrosion rates decreased to very low values (Figs. 3b and 4b) indicating the passivation of the zinc coatings in concrete matrix [4,6–15,17]. In particular, Fig. 4b shows a delay in the attainment of a passive corrosion potential for the bars embedded in specimens P, indicating a lower protection of the passive layer on the zinc coatings in contact with the more alkaline matrix.

Figs. 5 and 6 show that all the bars embedded in specimens P have corrosion rates higher than those related to specimens L both in tap water and in NaCl solution before the attack promoted by the chloride ions. This different behaviour must be attributed to the different passive layers formed on the coatings in the two concrete matrixes. Other authors [9,11] found that in aqueous solutions of $Ca(OH)_2$ the composition and the structure of the passive layer formed on galvanized steel depend on the pH of the alkaline environment in contact with the galvanized bars and on the concentration of Ca^{2+} ions. In particular, a passive layer composed of calcium hydroxyzincate, $Ca(Zn(OH)_3)_2 \cdot 2H_2O$ (CaHZn) was found to be formed in the pH range 11.5–13.2, while outside this range a less protective layer of ZnO and $Zn(OH)_2$ was observed [4]. Considering that the pH of the solution within the concrete pores is lower than 13.3, other authors [12] indicated that the corrosion product on galvanized bars are mainly formed of CaHZn, protective in the pH range 12–12.8 and less protective in the range 12.8–13.3. As a consequence of these remarks, very low corrosion rates can be expected if the interaction between the concrete matrix and the galvanized reinforcements produces with time a compact and continuous layer of CaHZn on the zinc coatings; on the contrary, in the presence of a discontinuous layer of CaHZn and/or in the presence of $Zn(OH)_2$ and ZnO, the corrosion rates could be significantly high. The pH in the pores of the more alkaline specimens P is higher than that of specimens L and thus probably leads to the formation of a less protective layer, which explains the higher corrosion rates found for the bars embedded in specimens P.

Independently from the nature of the concrete matrix, the presence of the "positive peaks" in correspondence of the wetting periods during wet–dry exposure, indicates that the passive layer formed on the galvanized reinforcements and on the pure zinc rods, during the air curing period, is not completely protective. This is probably due to the presence of ZnO and $Zn(OH)_2$ corrosion products in some zones of the reinforcements. The "damping phenomenon", observed in particular during wet–dry exposure with tap water, can be explained with the transformation of ZnO or $Zn(OH)_2$ into CaHZn, which becomes more and more compact and protective with the increasing number of wet–dry cycles, which slows down the corrosion rates (Figs. 5b and 6b). This transformation is in agreement with the results of other authors [19–21] who characterized the interfacial transition zone (ITZ) between the cement paste and the galvanized steel after 28 days of curing: they found the presence of the crystalline CaHZn, produced from the transformation of the $Zn(OH)_2$, that was not observed during the initial interaction between the two materials.

When the alkalinity of the concrete matrix is the only factor determining the corrosion of the galvanized bars (in the absence of chloride ions), the coatings obtained in the Zn–Ni–Sn–Bi bath are those with the highest corrosion rates, while the bars coated in the Zn–Pb and Zn–Ni–Bi baths showed similar behaviour and lower corrosion rates (Figs. 3–6). On the contrary, when the aggressiveness of the concrete matrix is determined mainly by the critical penetration of chlorides (in specimens L obtained with a low alkali cement), Zn–Ni–Sn–Bi coating was attacked only when the chloride concentration at the concrete cover depth reached the threshold of 4.02% (by weight of cement), which is higher than those necessary for the attack of the other two coatings studied (1.36% for Zn–Ni–Bi, 1.73% for Zn–Pb, Fig. 5a). Therefore, the bars obtained from Zn–Ni–Sn–Bi bath can be used in an environment contaminated by chlorides, for example on the sea front if they are embedded in a concrete manufactured with a low alkali cement.

It is noteworthy that the chlorides concentration threshold necessary for the attack initiation on the galvanized bar embedded in specimens L was in all cases significantly higher than that reported in the literature [6,22,23]. In the case of specimens P, the corrosion initiation on the different galvanized bars was not observed (Fig. 6a), even if the chloride content reached values for which the localized

corrosion initiated on the bars in specimens L (Fig. 5a). These results indicate that in a high alkali concrete, the chlorides concentration threshold for the localized corrosion initiation is higher than that of a low alkali concrete, in accordance with other authors [12,17]. Furthermore, the powder analysis and the $AgNO_3$ spraying test showed that the high alkali concrete is subjected to a lower chlorides penetration.

In all experimental conditions examined, the pure zinc rod showed the best corrosion resistance, even with a high contamination of chlorides (Fig. 5a). This result is in agreement with those of other authors in alkaline environments [12,17] and can be attributed to the presence of the alloying elements on the zinc coatings. This indicates that the presence of a uniform η phase on the top of the coatings leads to an improvement of the corrosion resistance in concrete.

The metallographic observations on the galvanized bars after wet–dry exposure in sodium chloride solution confirm the results of the corrosion tests: the chlorides attack was more severe and penetrating on the zinc coatings of the bars embedded in specimens L (Fig. 8a–c) with respect to that on the galvanized bars embedded in specimens P (Fig. 8d–f). On the contrary, considering the different bars in the same specimens type, L or P, the metallographic analysis is not always in agreement with the results of the corrosion tests. In fact, the coating obtained from Zn–Ni–Bi bath and embedded in specimens P appears the least attacked (Fig. 8e), as indicated also by corrosion rates measurements (Fig. 6a), while the coating obtained from Zn–Ni–Sn–Bi bath and embedded in specimens L does not appear the most resistant (Fig. 8c), as expected from the corrosion data (Fig. 5a). However, it is noteworthy that the initial thicknesses of the different coatings was not the same; in particular, the thicknesses of Zn–Ni–Sn–Bi coating was the lowest (Fig. 2). The microstructure of the galvanized bars after wet–dry exposure in tap water showed a less severe attack. Furthermore, these observations confirm the higher corrosion rates found for the bars in specimens P, with respect to those of the bars in specimens L. In this case, the high alkalinity of the concrete matrix obtained with cement P can be considered the only factor determining the corrosion of the galvanized bars.

5. Conclusions

The corrosion resistance of two different galvanized bars obtained respectively with a Zn–Ni–Bi and Zn–Ni–Sn–Bi "modified" baths was studied in comparison with the corrosion resistance of a bar galvanized with the "traditional" Zn–Pb bath and in comparison with the corrosion behaviour of a pure zinc rod. This study was performed in concrete specimens obtained with two cements of different alkalinity, by measuring the corrosion potential and by determining the corrosion rates during the air curing period and during wet–dry exposure both in tap water and in a 5% NaCl solution. At the end of the experimentation, the metallographic analysis was performed.

From this work, the following conclusions can be drawn:

- all galvanized bars always showed higher corrosion rates with respect to the pure zinc rod, due to the presence of alloying elements on the zinc coatings;
- the bars galvanized in the Zn–Ni–Sn–Bi bath are not suitable for high alkaline concrete matrix, while they showed a good corrosion behaviour when the dominant corrosion factor was the presence of chlorides: in the low alkali concrete matrix, localized corrosion initiation was observed only when 4.02% Cl^- by weight of cement at the concrete cover was reached;
- quite an opposite behaviour was observed for the bars galvanized in the Zn–Ni–Bi bath and in the Zn–Pb bath: in particular, in the low alkali concrete matrix the % Cl^- at concrete cover for localized corrosion initiation was 1.36 and 1.73 respectively;
- for the same or higher concentration of chlorides in correspondence of the concrete depth, the localized corrosion starts earlier in low alkali concrete matrix;
- the chlorides penetration was higher in the low alkali concrete matrix with respect to the high alkali concrete matrix;
- there was quite a good agreement with the corrosion test results and the metallographic observations of the coatings at the end of wet–dry exposure.

Acknowledgements

The authors are grateful to European Federation of Corrosion because this work was presented at EuroCorr 2005 (EFC event 233).

References

[1] Fratesi R, Ruffini N, Malavolta M, Bellezze T. Contemporary use of Ni and Bi in hot-dip galvanizing. Surf Coat Technol 2002;157:34–9.
[2] Richards RW, Clarke H. The influence of steel surface characteristics on galvanizing reactivity. EGGA, editor. Proceedings of the 17th international galvanizing conference. Paris: EGGA; 1994. p. GC7/1–GC7/12.
[3] Porter F. Zinc handbook. New York: Marcel Dekker Inc.; 1991.
[4] Yeomans SR, editor. Galvanized steel reinforcement in concrete. Oxford: Elsevier Sceince Ltd; 2004.
[5] Beguin Ph, Bosschaerts M, Dhaussy D, Pankert R, Gilles M. Galveco®, A solution for galvanizing reactive steel. EGGA, editor. Proceedings of the 19th international galvanizing conference. Berlin: EGGA; 2000. p. 1–7.
[6] Fratesi R. Hot-dip galvanized rebars for building construction. Industria Italiana del Cemento 1998;735(9):720–33.
[7] Macias A, Andrade C. Corrosion of galvanized steel reinforcements in alkaline solutions. Part 1: Electrochemical results. Br Corros J 1987;22(2):113–8.
[8] Macias A, Andrade C. Corrosion of galvanized steel reinforcements in alkaline solutions. Part 2: SEM study and identification of corrosion products. Br Corros J 1987;22(2):119–29.
[9] Macias A, Andrade C. Corrosion of galvanized steel in dilute $Ca(OH)_2$ solutions (pH 11.1–12.6). Br Corros J 1987;22(3):162–71.

[10] Macias A, Andrade C. Corrosion rate of galvanized steel immersed in saturated solutions of $Ca(OH)_2$ in the pH range 12–13.8. Br Corros J 1983;18(2):82–7.
[11] Blanco MT, Andrade C, Macias A. SEM study of the corrosion products of galvanized reinforcements immersed in solutions in the pH range 12.6–13.6. Br Corros J 1984;19(1):41–8.
[12] Andrade MC, Macias A. Galvanized reinforcements in concrete. In: Wilson AD, Nichols JW, Prosser HJ, editors. Surface coatings-2. New York: Elsevier Applied Science; 1988. p. 137–82.
[13] Fratesi R, Moriconi G, Bellezze T, Tittarelli F. Influence of cement alkalinity on corrosion of galvanized steel bars in concrete. Basheer PAM, Sloan TD, editors. Proceedings of the COST 521 workshop. Belfast: The Queen's University of Belfast; 2000. p. 45–52.
[14] Fratesi R, Moriconi G, Bellezze T, Tittarelli F. The effect of cement alkalinity on zinc coating durability of galvanized steel bars in concrete. In: Mattila J, editor. Proceedings of the COST 521 workshop. Tampere: Department of Civil Engineering; 2001. p. 55–60.
[15] Bellezze T, Coppola L, Fratesi R. Evaluation of hexavalent chromium-free passivation treatment of galvanized bars for reinforced concrete. In: Malhotra VM, editor. Proceedings of the fifth CANMET/ACI international conference on ''Durability of Concrete'', vol. 1. Barcelona: American Concrete Institute; 2000. p. 573–89.
[16] Stern M, Geary AL. Electrochemical polarization—I. A theoretical analysis of the shape of polarization curves. J Electrochem Soc 1957;104(1):56–63.
[17] Alonso C, Sánchez J, Fullea J, Andrade C. The addition of nickel to improve the corrosion resistance of galvanized reinforcement. EGGA, editor. Proceedings of the 19th international galvanizing conference. Berlin: EGGA; 2000. p. 1–8.
[18] Berke NS, Shen DF, Sundberg KM. Comparison of the polarization resistance technique to the macrocell corrosion technique. In: Corrosion Rates of Steel in Concrete, Berke N.S., Chaker V., Whiting D, editors. Philadelphia: ASTM STP 1065; 1990. p. 38–51.
[19] Duval R, Arliguie MG. Passivation du zinc dans l'hydroxyde de calcium, en égard au comportament de l'ancier galvanisé dans le beton. Mémoires Scintifique Rev Métallurg 1974;71(11):719–27.
[20] Arliguie G, Ollivier JP, Grandet J. Etude de l'effet retardateur du zinc sur l'hydratation de la pate de ciment portland. Cement Concr Res 1982;12(1):79–86.
[21] Belaïd F, Arliguie G, François R. Porous structure of the ITZ around galvanized and ordinary steel reinforcements. Cement Concr Res 2001;31(11):1561–6.
[22] Pedeferri P, Bertolini L. La corrosione nel calcestruzzo e negli ambienti naturali. Milano: McGraw-Hill; 1996.
[23] Yeomans SR. Performance of black, galvanized and epoxy-coated reinforcing steels in chloride-contaminated concrete. Corrosion 1994;50(1):72–81.